NuSol — Numerical solver for the 3D stationary nuclear Schrödinger equation☆

Timo Graen, Helmut Grubmüller *

Max Planck Institute for Biophysical Chemistry, Am Fassberg 11, 37073 Göttingen, Germany

ABSTRACT

The classification of short hydrogen bonds depends on several factors including the shape and energy spacing between the nuclear eigenstates of the hydrogen.

Here, we describe the NuSol program in which three classes of algorithms were implemented to solve the 1D, 2D and 3D time independent nuclear Schrödinger equation. The Schrödinger equation was solved using the finite differences based Numerov's method which was extended to higher dimensions, the more accurate pseudo-spectral Chebyshev collocation method and the *sinc* discrete variable representation by Colbert and Miller. NuSol can be applied to solve the Schrödinger equation for arbitrary analytical or numerical potentials with focus on nuclei bound by the potential of their molecular environment. We validated the methods against literature values for the 2D Henon–Heiles potential, the 3D linearly coupled sextic oscillators and applied them to study hydrogen bonding in the malonaldehyde derivate 4-cyano-2,2,6,6-tetramethyl-3,5-heptanedione.

With NuSol, the extent of nuclear delocalization in a given molecular potential can directly be calculated without relying on linear reaction coordinates in 3D molecular space.

Program summary

Program title: NuSol

Catalogue identifier: AEXO_v1_0

Program summary URL: http://cpc.cs.qub.ac.uk/summaries/AEXO_v1_0.html

Program obtainable from: CPC Program Library, Queen's University, Belfast, N. Ireland

Licensing provisions: GPL 3.0

No. of lines in distributed program, including test data, etc.: 195332

No. of bytes in distributed program, including test data, etc.: 4489808

Distribution format: tar.gz

Programming language: Python 2.7, C.

Computer: PC.

Operating system: Linux.

RAM: 0.1–40 GB

Classification: 16.1.

External routines: FEAST v2.1 [1][2] (included in the distribution file).

Nature of problem: Solving the 3D nuclear Schrödinger Equation

Solution method: Grid solver based on Numerov's method, Chebyshev collocation and *sinc*() DVR for 1D/2D/3D potential grids

Running time: System dependent

References:

[1] E. Polizzi, Density-Matrix-Based Algorithms for Solving Eigenvalue Problems, Phys. Rev. B. Vol. 79, 115112 (2009)
[2] E. Polizzi, A High-Performance Numerical Library for Solving Eigenvalue Problems: FEAST solver User's guide, arxiv.org/abs/1203.4031 (2012).

1. Introduction

Hydrogen bonds represent important interactions in inorganic, organic and biomolecules [1]. Intramolecular hydrogen bonds often connect distant parts of a molecule, thereby stabilizing molecular structure. Of particular interest are short intramolecular O–H$\cdots$O hydrogen bonds for their presence in enzyme [2,3] and photo centers [4–7]. The energetics of these bonds is determined by the nuclear motion of the involved hydrogen atom. Methods suitable to solve the nuclear eigenfunctions of the hydrogen have been around for a long time in nuclear physics but freely available implementations suitable for molecular potentials are rare. These methods most commonly rely on – but are not limited to – harmonic oscillator basis functions or plane wave discrete variable representation (DVR), as recently reviewed by Bulgac et al. [8] and by Light and Carrington [9].

In this work, the Nuclear Solver (NuSol) program is introduced. NuSol enables accurate and reproducible nuclear wave function calculations of single particles in arbitrary bound analytical or numerically scanned molecular potentials. Three classes of solvers are made available. First, the finite differences approach of Numerov [10,11] was extended to two and three dimensions and implemented. To our knowledge, no explicit generalization of the Numerov method to higher dimensions has been published in the literature other than partial extensions [12,13]. Second, a high accuracy Chebyshev pseudo-spectral collocation algorithm [14] was implemented which benefits from the exponential convergence while being more sparse in the center of the grid. In applications with more than one nucleus, this feature can be beneficial because it is less expensive to calculate the full numerical coupling potential in regions of high nuclear density. Third, the powerful *sinc*() discrete variable representation (DVR) by Colbert and Miller [15] was implemented which likely is the method of choice for most practical NuSol applications for its speed and accuracy.

The NuSol program makes the finite differences based Numerov, the pseudo-spectral Chebyshev method and the *sinc*() DVR easily accessible to anyone interested in solving the Schrödinger equation for single nuclei and especially for studying hydrogen bonding via user defined analytical potentials or scanned molecular potentials from quantum chemical calculations.

2. Methods

2.1. Task

The Numerov method is a solver for the one-dimensional stationary Schrödinger equation. Here, we extend the method to two and three dimensions and derive the corresponding generalized eigenvalue equations.

2.2. 1D Numerov algorithm

To clarify the notation, we first summarize the one dimensional Numerov method. The method solves the Schrödinger equation

$$\triangle \psi = -f\psi \tag{1}$$

with

$$f = \frac{2m}{\hbar^2}(E - V) \tag{2}$$

by discretizing the second derivative $\triangle$ on a grid. The simplest such approximation for the second derivative is

$$\triangle \psi(x) \approx \frac{\psi(x+h) - 2\psi(x) + \psi(x-h)}{h^2} + \mathcal{O}(h^4) \tag{3}$$

where h is the grid spacing and the error term is of order $\mathcal{O}(h^2)$.

The Numerov algorithm includes higher order terms into this expansion. This is achieved by first adding a forward and backward Taylor expansion of $\psi(x)$ up to order $\mathcal{O}(h^6)$, followed by a reinsertion of the identity (1) in order to reduce the fourth order derivative to second order as

$$h^2 \triangle \psi(x) \approx \psi(x+h) - 2\psi(x) + \psi(x-h) + \frac{h^4}{12}\frac{d^2(f\psi)}{dx^2} + \mathcal{O}(h^6). \tag{4}$$

As the number of such finite difference terms increases rapidly with dimensionality, the following shorthand notation for grid point indices is used:

$$\psi(x_n) = \psi_n \quad \text{and} \quad \psi(x_n \pm h) = \psi_{n\pm}.$$

After rewriting the terms, the Numerov algorithm can be obtained by approximating the second derivative in Eq. (4) with Eq. (3) and reinserting Eq. (1),

$$\psi_{n_+} - 2\psi_n + \psi_{n_-} = -\frac{h^2}{12}\left(f_{n_+}\psi_{n_+} + 10f_n\psi_n + f_{n_-}\psi_{n_-}\right) + \mathcal{O}(h^6). \tag{5}$$

This is the one dimensional numerical stencil for an equally spaced grid of N points and implicit Dirichlet boundary condition at $\psi_0 = \psi_N = 0$. When applied to a grid, Eq. (5) is a generalized eigenvalue problem which can efficiently be solved for the lowest energy eigenvalues and eigenvectors using the FEAST [16,17] or ARPACK-NG[1] algorithms. These solvers are more robust than the shooting method [18] for solving the eigenvalue problem as they do not depend on good initial guess vectors close to the eigenvector of interest. The FEAST algorithm makes use of contour integration techniques to find eigenvalues within a specified energy range, whereas the ARPACK-NG routines belong to the class of Krylov subspace methods. The resulting eigenvalues and eigenvectors are the solution of the Schrödinger equation.

2.3. 2D Numerov algorithm

The two dimensional Numerov method is derived in the following section for the two dimensional Schrödinger equation

$$\left(\frac{d^2}{dx_1^2} + \frac{d^2}{dx_2^2}\right)\psi(x_1, x_2) = -f(x_1, x_2)\psi(x_1, x_2), \tag{6}$$

with $f(x_1, x_2) = \frac{2m}{\hbar^2}(E - V(x_1, x_2))$. The derivation begins analogously to the 1D case by summing the four 2D Taylor expansion around $(x_1^0 \pm h_{x_1}, x_2^0 \pm h_{x_2})$ with equal grid spacing in all dimensions $h = h_{x_1} = h_{x_2}$. Grid points are now indexed using $\psi_{n\pm,k\pm}$ instead of $\psi_{n\pm}$.

Only even powers of h remain while the odd powers cancel,

$$\psi_{n_+,k_+} + \psi_{n_+,k_-} + \psi_{n_-,k_+} + \psi_{n_-,k_-} = 4\psi + \frac{4h^2}{2!}\left(\frac{d^2\psi}{dx_1^2} + \frac{d^2\psi}{dx_2^2}\right) + \frac{4h^4}{4!}\left(\frac{d^4\psi}{dx_1^4} + 6\frac{d^4\psi}{dx_1^2dx_2^2} + \frac{d^4\psi}{dx_2^4}\right) + \mathcal{O}(h^6).$$

The remaining terms are now simplified using Eq. (6) in analogy to the 1D Numerov case,

$$\left(\frac{d^4\psi}{dx_1^4} + 2\frac{d^4\psi}{dx_1^2dx_2^2} + \frac{d^4\psi}{dx_2^4}\right) = -\frac{d^2(f\psi)}{dx_1^2} - \frac{d^2(f\psi)}{dx_2^2}$$

and the second derivatives are again approximated by the finite difference equation (3). This, again, results in many similar finite difference expansion terms involving $\psi_{n\pm,k\pm}$. To make the derivation more transparent, a stencil notation is introduced which removes the $\psi_{n\pm,k\pm}$ terms and positions the remaining factors according to the stencil indices $n\pm, k\pm$ as

$$\begin{matrix} a_{11}\psi_{n_+,k_-} & +a_{12}\psi_{n_+,k} & +a_{13}\psi_{n_+,k_+} \\ +a_{21}\psi_{n,k_-} & +a_{22}\psi_{n,k} & +a_{23}\psi_{n,k_+} \\ +a_{31}\psi_{n_-,k_-} & +a_{32}\psi_{n_-,k} & +a_{33}\psi_{n_-,k_+} \end{matrix} = \begin{pmatrix} a_{11} & a_{12} & a_{13} \\ a_{21} & a_{22} & a_{23} \\ a_{31} & a_{32} & a_{33} \end{pmatrix}'$$

and denoted by dashed matrix parentheses. The remaining fourth order derivative term was expanded and presented in stencil notation as

$$h^4\frac{d^4\psi}{dx_1^2dx_2^2} \approx \begin{pmatrix} 1 & -2 & 1 \\ -2 & 4 & -2 \\ 1 & -2 & 1 \end{pmatrix}'.$$

The two dimensional analog to the 1D Numerov is obtained by reinserting all of the above terms which results in

$$\begin{pmatrix} 1 & 4 & 1 \\ 4 & -20 & 4 \\ 1 & 4 & 1 \end{pmatrix}' = \frac{-h^2}{2}\begin{pmatrix} & f_{n_+,k} & \\ f_{n,k_-} & 8f_{n,k} & f_{n,k_+} \\ & f_{n_-,k} & \end{pmatrix}',$$

after which the f operator is reinserted. This yields the stencil for the 2D Numerov solver:

$$\frac{-\hbar^2}{mh^2}\begin{pmatrix} 1 & 4 & 1 \\ 4 & -20 & 4 \\ 1 & 4 & 1 \end{pmatrix}' + \begin{pmatrix} & V_{n_+,k} & \\ V_{n,k_-} & 8V_{n,k} & V_{n,k_+} \\ & V_{n_-,k} & \end{pmatrix}' = E\begin{pmatrix} & 1 & \\ 1 & 8 & 1 \\ & 1 & \end{pmatrix}'. \tag{7}$$

The eigenvectors and eigenvalues of this stencil applied to a 2D grid are again the eigenfunction and energy eigenvalues of the Schrödinger equation, respectively.

---

[1] https://github.com/opencollab/arpack-ng.

2.4. 3D Numerov algorithm

The 3D solver is derived in close analogy to the 2D case.

The eight 3D Taylor expansions $\psi(x_1^0 \pm h_{x_1}, x_2^0 \pm h_{x_2}, x_3^0 \pm h_{x_3})$ around (x_1^0, x_2^0, x_3^0) were added up including terms of order h^5 or lower. Most terms cancel, leaving only even powers in h,

$$
\begin{aligned}
&\psi_{n_+,k_+,l_+} \quad +\psi_{n_-,k_+,l_+} \quad +\psi_{n_+,k_-,l_+} \quad +\psi_{n_+,k_-,l_-}+ \\
&\psi_{n_+,k_+,l_-} \quad +\psi_{n_-,k_+,l_-} \quad +\psi_{n_-,k_-,l_-} \quad +\psi_{n_-,k_-,l_+} \\
&= 8\psi + \frac{8h^2}{2!}\left(\frac{d^2\psi}{dx_1^2} + \frac{d^2\psi}{dx_2^2} + \frac{d^2\psi}{dx_3^2}\right) + \frac{8h^4}{4!}\left(\frac{d^4\psi}{d^4x_1} + \frac{d^4\psi}{d^4x_2} + \frac{d^4\psi}{d^4x_3}\right) + \frac{48h^4}{4!}\left(\frac{d^4\psi}{d^2x_1d^2x_2} + \frac{d^4\psi}{d^2x_1d^2x_3} + \frac{d^4\psi}{d^2x_2d^2x_3}\right).
\end{aligned}
$$

Due to the increased dimensionality, the stencil was sliced into a sum of $l-$, l and $l+$ slices to better visualize the tensor elements. Similar to the 2D case, the derivatives were approximated,

$$
-\frac{1}{h^2}\left[\begin{pmatrix} 3 & -4 & 3 \\ -4 & 16 & -4 \\ 3 & -4 & 3 \end{pmatrix}'_{l-} + \begin{pmatrix} -4 & 16 & -4 \\ 16 & -72 & 16 \\ -4 & 16 & -4 \end{pmatrix}'_{l} + \begin{pmatrix} 3 & -4 & 3 \\ -4 & 16 & -4 \\ 3 & -4 & 3 \end{pmatrix}'_{l+} \right]
$$

$$
= \begin{pmatrix} & & \\ & f_{n,k} & \\ & & \end{pmatrix}'_{l-} + \begin{pmatrix} & f_{n_+,k} & \\ f_{n,k_-} & 6f_{n,k} & f_{n,k_+} \\ & f_{n_-,k} & \end{pmatrix}'_{l} + \begin{pmatrix} & & \\ & f_{n,k} & \\ & & \end{pmatrix}'_{l+}
$$

and the f operator was reinserted into the equation. The final working form of the 3D Numerov solver reads:

$$
-\frac{\hbar^2}{2mh^2}\left[\begin{pmatrix} 3 & -4 & 3 \\ -4 & 16 & -4 \\ 3 & -4 & 3 \end{pmatrix}'_{l-} + \begin{pmatrix} -4 & 16 & -4 \\ 16 & -72 & 16 \\ -4 & 16 & -4 \end{pmatrix}'_{l} + \begin{pmatrix} 3 & -4 & 3 \\ -4 & 16 & -4 \\ 3 & -4 & 3 \end{pmatrix}'_{l+} \right]
$$

$$
+ \left[\begin{pmatrix} & & \\ & V_{n,k} & \\ & & \end{pmatrix}'_{l-} + \begin{pmatrix} & V_{n_-,k} & \\ V_{n,k_-} & 6V_{n,k} & V_{n,k_+} \\ & V_{n_+,k} & \end{pmatrix}'_{l} + \begin{pmatrix} & & \\ & V_{n,k} & \\ & & \end{pmatrix}'_{l+} \right]
$$

$$
= E \left[\begin{pmatrix} & & \\ & 1 & \\ & & \end{pmatrix}'_{l-} + \begin{pmatrix} & 1 & \\ 1 & 6 & 1 \\ & 1 & \end{pmatrix}'_{l} + \begin{pmatrix} & & \\ & 1 & \\ & & \end{pmatrix}'_{l+} \right]. \tag{8}
$$

2.5. Chebyshev solver

In addition to the Numerov solver, NuSol also implements the exponentially convergent Chebyshev collocation, or pseudo-spectral, method. A review of the method is provided in the book of Fornberg [19], and a more recent derivation by Mason and Handscomb [14]. In this method, the eigenfunctions of Eq. (1) are approximated by an order N Chebyshev polynomial $T_N(x)$ on the interval $[-1, 1]$ and evaluated at the $N + 1$ zeros y_i of polynomial $T_{N+1}(x)$. The core of the solver is to approximate the differentiation matrix at the collocation points y_i

$$
\mathbf{D} = \begin{pmatrix}
\frac{1}{6}(1 + 2N^2) & -2\frac{1}{1-y_1} & 2\frac{1}{1-y_2} & \cdots & 2\frac{(-1)^{N-1}}{1-y_{N-1}} & 0.5(-1)^N \\
0.5\frac{1}{1-y_1} & -0.5\frac{y_1}{1-y_1^2} & -\frac{1}{y_1-y_2} & \cdots & \frac{(-1)^{N-2}}{y_1-y_{N-1}} & 0.5\frac{(-1)^{N-1}}{1+y_1} \\
-0.5\frac{1}{1-y_2} & -\frac{1}{y_2-y_1} & 0.5\frac{y_2}{1-y_2^2} & \cdots & \frac{(-1)^{N-3}}{y_2-y_{N-1}} & 0.5\frac{(-1)^{N-2}}{1+y_2} \\
\vdots & \vdots & \vdots & \ddots & \vdots & \vdots \\
-0.5\frac{(-1)^{N-1}}{1-y_{N-1}} & \frac{(-1)^{N-2}}{y_{N-1}-y_1} & \frac{(-1)^{N-3}}{y_{N-1}-y_2} & \cdots & -0.5\frac{y_{N-1}}{1-y_{N-1}^2} & -0.5\frac{1}{1+y_{N-1}} \\
-0.5(-1)^N & -2\frac{(-1)^{N-1}}{1+y_1} & -2\frac{(-1)^{N-2}}{1+y_2} & \cdots & 2\frac{1}{1+y_{N-1}} & -\frac{1}{6}(1+2N^2)
\end{pmatrix}.
$$

The differentiation matrix $\mathbf{D}$ is inserted into Eq. (1)

$$
\left[\frac{-\hbar^2}{2m}\mathbf{D}^2 + \mathbf{V}_{y_N}\right]\psi_{y_N} = E\psi_{y_N} \tag{9}
$$

where V_{y_N} is a diagonal potential matrix at the collocation points y_i. Eq. (9) is a large eigenvalue equation for which the first eigenvectors and eigenvalues can be solved iteratively. Two and three dimensional solutions are calculated in NuSol via the Kronecker sum of the differentiation matrix and the unit matrix $\mathbf{E}_N$ as

$$
\mathbf{D}_2 = \mathbf{D} \otimes \mathbf{E}_N + \mathbf{E}_N \otimes \mathbf{D}
$$

Table 1
Validation of the 2D NuSol solvers against the Henon–Heiles potential. The eigenvalues for the first 10 eigenstates of the Henon–Heiles potential are shown. Energies for degenerate states are shown were applicable.

E	Reference Braun [20]	This work Chebyshev $N = 50$	This work DVR $dh = 0.1$	This work Numerov $dh = 0.1$
E_0	0.998595	Same	Same	0.998594
E_1	1.990077	Same	Same	1.990075
	1.990077	Same	Same	1.990075
E_2	2.956243	Same	Same	2.956237
E_3	2.985326	Same	Same	2.985318
	2.985326	Same	Same	2.985325
E_4	3.925964	Same	Same	3.925950
	3.925964	Same	Same	3.925951
E_5	3.982417	Same	Same	3.982407
E_6	3.985761	Same	Same	3.985751
E_7	4.870144	Same	Same	4.870120
E_8	4.898644	Same	Same	4.898606
	4.898644	4.898645	Same	4.898636
E_9	4.986251	Same	Same	4.986232
	4.986251	Same	Same	4.986232
E_{10}	5.817019	5.817020	Same	5.816980
	5.817027	5.817028	5.817024	5.816983

$$\mathbf{D}_3 = \mathbf{D} \otimes \mathbf{E}_N \otimes \mathbf{E}_N + \mathbf{E}_N \otimes \mathbf{D} \otimes \mathbf{E}_N + \mathbf{E}_N \otimes \mathbf{E}_N \otimes \mathbf{D}. \tag{10}$$

The potential $\mathbf{V}_{y_N}$ remains diagonal for higher dimensions.

2.6. sinc() DVR solver

NuSol also implements the *sinc*() DVR method described by Colbert and Miller [15] which operates on equally spaced grids on the domain $(-\infty, \infty)$ like the Numerov algorithm. In contrast to the Numerov algorithm, the method does not truncate the expansion, but rather describes the finite differences approximation to infinite order using an infinite basis of *sinc*() functions evaluated at the grid points analytically. This provides increased accuracy, and the matrix elements

$$D^2_{i,i'} = \frac{\hbar^2 (-1)^{(i-i')}}{2mh^2} \begin{cases} \pi^2/3, & i = i' \\ \dfrac{2}{(i-i')^2}, & i \neq i' \end{cases} \tag{11}$$

of the $\mathbf{D}^2$ matrix from Eq. (9) are easier to calculate. Higher dimensional solvers are constructed using the Kronecker products of Eq. (10).

2.7. Comparison to reference calculations

The accuracy of the discussed Numerov, Chebyshev and DVR implementations was assessed by comparing results with two reference systems from the literature, the 2D chaotic Henon–Heiles potential and the 3D linearly coupled sextic oscillators.

The Henon–Heiles potential

$$V(x, y) = \frac{1}{2}(x^2 + y^2) + \frac{1}{4\sqrt{5}} x \left(y^2 - \frac{1}{3} x^2 \right), \tag{12}$$

was solved on a grid with dimensions $x = [-6, 6]$ and $y = [-6, 6]$ using a grid spacing of $\Delta h = 0.1$ for the Numerov and DVR, and $N = 50$ collocation points for the Chebyshev solver. The resulting eigenvalues are shown in Table 1 together with reference solutions from the Chebyshev–Lanczos algorithm of Braun et al. [20].

The ground and excited state Numerov energies correspond well with their reference values, yielding a relative error of order 10^{-6}–10^{-5}. The Chebyshev and DVR algorithms, as expected, performed significantly better, recovering the results of Braun et al. up to the last reported digits.

Next, we evaluated the performance of the solvers for a more realistic three dimensional coupled model system. To this end, the energy eigenvalues of the tree linearly coupled sextic oscillator system with the potential

$$V(x, y, z) = \frac{1}{2}x^2 + 2x^4 + \frac{1}{2}x^6 + \frac{1}{2}y^2 + 2y^4 + \frac{1}{2}y^6 + \frac{1}{2}z^2 + 2z^4 + \frac{1}{2}z^6 + xy + yz + xz$$

were calculated. All solutions were obtained using a grid with dimensions $x = [-4, 4]$, $y = [-4, 4]$, $z = [-4, 4]$ at varying numbers of grid and collocation points N in the range of $N = 15$ to $N = 40$. Here, $N = 40$ requires 64.000 grid points which roughly corresponds to the largest grid sizes feasible when the potentials are scanned using quantum chemical methods. Fig. 1 shows the relative errors $|E_{calc} - E_{ref.}|/E_{ref.}$ of eigenstates E_0, E_4 and E_9 with respect to their reference values. The reference values were again taken from the high accuracy Chebyshev–Lanczos results reported by Braun et al. [20]. The results show the slow but predictable convergence behavior of the Numerov solver which robustly recovers the first few digits of the reference solution already at sparse grid resolutions of $N \approx 25$. However, the superior convergence of the Chebyshev and especially the DVR implementation clearly outperforms the Numerov method. Only in the narrow window of $N < 25$ and for high excited states, does Numerov perform better than the Chebyshev method due to the low collocation point density at the center of the potential. In summary, the *sinc*() DVR was found superior in all tested cases.
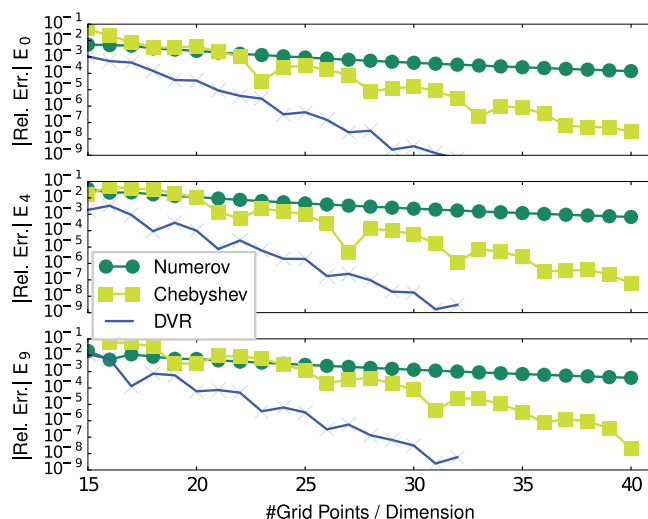
Fig. 1. Coupled 3D Sextic Oscillators Scaling. The relative errors of eigenvalues E_0 (top), E_4 (middle) and E_9 (bottom) are shown for the Numerov [filled green circle], Chebyshev [filled yellow square] methods and $sinc()$ DVR [blue lines]. Reference values were taken from the high accuracy Chebyshev–Lanczos calculations of Braun et al. [20].
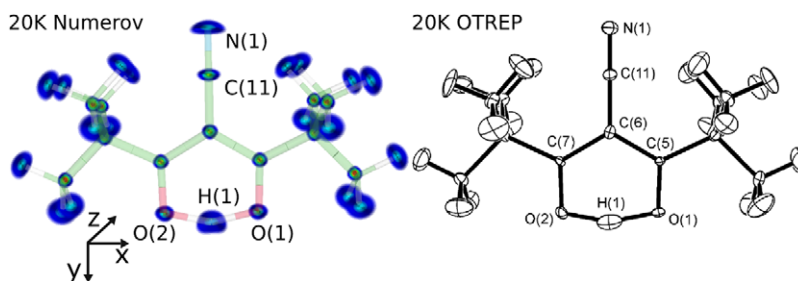

Fig. 2. Application of NuSol to 4-cyano-2,2,6,6-tetramethyl-3,5-heptanedione. NuSol was used to calculate the Boltzmann weighted eigenstates of the uncoupled individual atoms for a temperature of 20 K. The figure shows the molecular structure in stick representation with overlayed wave function densities (left). The 20 K neutron scattering OTREP* plot of Belot et al. [21] is shown for reference (right).
Source: * Reprinted (Fig. 1) 'OTREP plot of the neutron structure' with permission from J. Phys. Chem. B, 2004, 108 (22), pp 6922–6926 http://dx.doi.org/10.1021jp0496710. © 2015, American Chemical Society.

2.8. Application to O–H· · ·O hydrogen bonds

In the previous section, two model systems were solved to assess the accuracy of the implemented algorithms. We now focus on the application of NuSol, the solution of the nuclear Schrödinger equation for molecular potentials obtained from quantum chemical calculations. In the following, the malonaldehyde derivative, 4-cyano-2,2,6,6-tetramethyl-3,5-heptanedione as characterized by Belot et al. [21], was studied.

Belot et al. suggested a low-barrier double-well hydrogen bond (LBDWHB) for hydrogen H(1). This bond type was defined for double well potentials with an energy barrier of approximately 6 kJ/mol. The ground state wave function was described to be bimodal and located just below the energy barrier. A small energy gap to the excited state above the barrier would allow for significant thermal occupation and therefore delocalization into the center of the potential. Here, NuSol was used to calculate the corresponding H(1) nuclear wave functions and energies in order to compare them to this definition of a LBDWHB.

NuSol was used to solve the nuclear Schrödinger equation for each atom individually. A set of scans was performed on cubic grids located at the nuclear positions reported by Belot et al. A cubic grid with a length of 2.4 Bohr and $N = 25$ grid points per dimension was used. The proton mass in Hartree atomic units m_p/m_e was taken from the NIST CODATA Internationally recommended 2014 values of the fundamental physical constantsdatabase [22]. The resulting nuclear eigenvectors (Fig. 2) are shown as Boltzmann weighted superpositions corresponding to a temperature of 20 K. As can already be seen in this first sparse scan, the malonaldehyde derivative has a symmetric shared hydrogen bond located at position H(1) which is also visible in the OTREP plot of Belot et al. shown as reference.

Next, the grid resolution of atom H(1) was increased to obtain a more accurate description of the potential. A dense $\Delta h = 0.05$ Bohr spaced grid was used with dimensions $x = [-1.0, 1.0]$, $y = [-0.5, 1.1]$, $z = [-0.85, 0.85]$ Bohr and $N = 41 \times 33 \times 35$ grid-/collocation-points. The nuclear coordinates were not optimized prior to the grid scan for better reproducibility in future works. However, the error introduced by this choice of slightly asymmetric experimental coordinates was assessed in an additional scan on the symmetrized geometry, see SI for details. All calculations were performed using the long-range and dispersion corrected wB97XD [23,24] DFT functional and a 6−31+G** basis set as implemented in the GAUSSIAN09 [25] program. Fig. 3 (bottom) shows a two dimensional slice of the H(1) double well potential. The dotted line follows the minimum energy pathway across the barrier of the double well which is plotted above. The energy barrier was previously calculated at the B3LYP level of theory by Hargis et al. [26] to be 1.59 kJ/mol and afterwards scaled to 4.27 kJ/mol using a correction factor. In this work, a barrier height of 2.64 kJ/mol was calculated for the unoptimized coordinates.

Using the three dimensional potential described above, Numerov, Chebyshev and DVR energies and wave functions were calculated. The lowest ten energies are shown in Table 2 together with the first three Numerov eigenvectors. Three important features are visible.
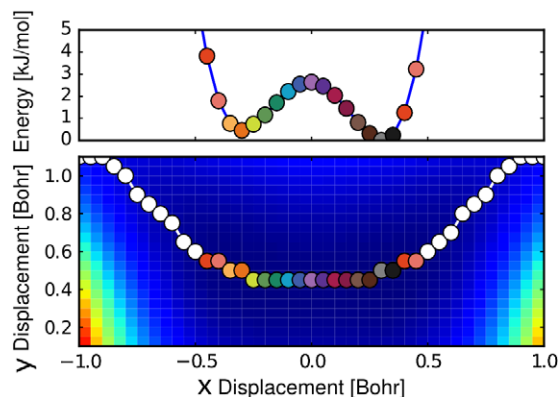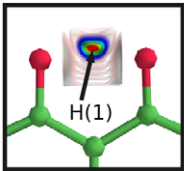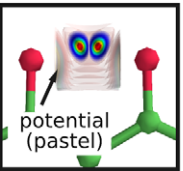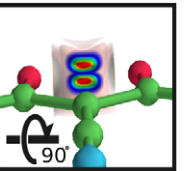
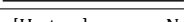**Fig. 3.** Potential of the minimum energy pathway of H(1) minimum energy pathway through the 3D double well potential of hydrogen H(1) is shown in the *x*–*y*-plane at $z = 0.0$ (bottom) together with the energy barrier along the path (top). The coordinate system matches that of Fig. 2 and the origin is located at the central position between the two oxygens O(1) and O(2). Color filled circles (bottom) indicate the positions of the energy values of the double well potential (top).

Table 2
H(1) Eigenfunction and Eigenvalues. The eigenvalues for the first ten eigenstates of the $H(1)$ were calculated with the Numerov, Chebyshev and DVR method. Figures E_0, E_1, E_2 (top) depict the first three Numerov eigenfunctions in the pastel color potential contour lines. Prior to the calculations, the Chebyshev potential energy grid was shifted to the minimum of the Numerov/DVR grid.

[Hartree]	Numerov	DVR	Chebyshev
E_0	0.009039419	0.009041598	0.009065707
E_1	0.012672791	0.012677814	0.012731550
E_2	0.014669929	0.014677108	0.014752613
E_3	0.016693694	0.016710929	0.016875048
E_4	0.017737312	0.017749351	0.017876106
E_5	0.019376101	0.019387952	0.019502058
E_6	0.020383723	0.020414260	0.020695568
E_7	0.020744253	0.020770146	0.021022052
E_8	0.021958508	0.021982862	0.022220025
E_9	0.023057705	0.023097686	0.023476907

First, the ground state wave function with energy $E_{0,Numerov} = 23.7$ kJ/mol is single modal and located well above the energy barrier of 2.6 kJ/mol. Second, the spacing between E_0 and E_1 is larger than the thermal energy $E = k_B T$ available to the system at 300 K which results in a ground state occupation of $\approx$98%. Third, the independently calculated Numerov/DVR and Chebyshev ground state energies lie within only $\Delta E = 0.07$ kJ/mol of each other despite the differences in the underlying methods.

Within the level of approximation of our calculations, the suggested definition of a LBDWHB with a ground state energy closely below the barrier and significant thermal occupation into excited states above the barrier was not observed. Instead, a single modal ground state wave function was identified in a low barrier double well potential which lies far above the energy barrier with a large excited state energy gap. We can conclude that the NuSol results for H(1) are consistent with a low barrier double well hydrogen bond but the ground state energy was found to be above the barrier.

3. Program description

The NuSol program reads all run parameters from a config file provided by the user in a command line call:

Listing 1: Program call in Bash

```
python NuSol.py config.cfg
```

An interactive install script is located in the main NuSol folder which checks and installs the required dependencies. An annotated config_example.cfg is provided in the NuSol folder which describes the program commands. The config parser feeds the user input to the NuSol program as illustrated in the NuSol flow diagram of Fig. 4. Four solvers can be selected, the primitive $\mathcal{O}(h^2)$ solver of Eq. (3), the Numerov solvers of Eqs. (5), (7), (8), the Chebyshev solver described in Eq. (9) and the DVR method described in Eq. (11). The user can either specify an analytical potential or provide a Numpy object for a scanned molecular potential.
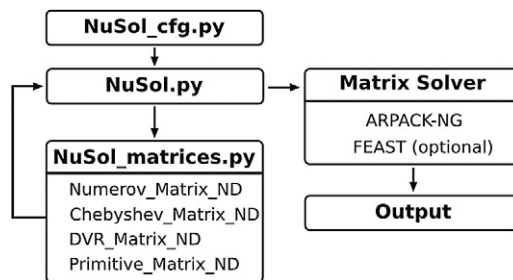
Fig. 4. Simple NuSol program overview. A user specified config file is parsed which in return creates the NuSol matrices corresponding to the specified method and potential parameters. The NuSol matrices are solved using the Numpy ARPACK-NG interface but can be changed to FEAST for parallel calculations.

Listing 2: NuSol Config Method and Potential Selection

```
# Method: Primitive, Numerov, DVR
#         Chebyshev, Chebyshev_Write_Grid_Only
METHOD         :     Numerov

# Read zero shifted POTENTIAL
# in numpy format .npy [Hartree]
POTENTIAL_PATH : ./harmonicOscillator.npy

# (OPTIONAL) user defined analytical potential
# Overrides potential specified in POTENTIAL\_PATH
# numpy functions are supported via np.function()
USER_FUNCTION  : 0.5 * (np.power(x,2.) + np.power(y,2.))

# Number of eigenvalues to calculate
N_EVAL         :     10
```

Further config parameters set the grid dimensions NDIM and particle properties which are described in more detail in the annotated example_config.cfg file. In the simplest case of NDIM=1, the Numerov/DVR grids are evenly spaced with NGRIDX points on the closed interval [*XMIN*, *XMAX*]. Higher grid dimensions are treated analogously. If the Chebyshev method is specified, the user defined grid is mapped onto the closed interval [−1, 1] using NGRIDX unevenly spaced collocation points. Prior to a Chebyshev calculation, the collocation grid can be written to disk by specifying Chebyshev_Write_Grid_Only in the METHODS section. In case the POTENTIAL_PATH option is used, the molecular potential needs to be scanned at these exact grid points beforehand. Each run will calculate N_EVAL lowest eigenvalues and eigenvectors.

The diagonalization of the NuSol Numerov matrices generated from the config parameters can either be performed using the build in Numpy ARPACK-NG interface, or the external FEAST library. The FEAST interface can handle very large sparse matrices on multiple processors but requires the proprietary Intel MKL library, which may not be available for all users. Therefore, the default solver is ARPACK-NG and FEAST is only used if the Numerov method is specified and the Intel MKL is found in the LD_LIBRARY_PATH system variable.

The eigenvectors and eigenvalues are written to disk in the user defined locations EIGENVALUES_OUT and EIGENVECTORS_OUT.

Listing 3: NuSol Config Output Files

```
EIGENVALUES_OUT : ./eval.dat
EIGENVECTORS_OUT: ./evec.dat
```

3.1. Example runs

The examples/folder in the NuSol directory contains config files for the Henon–Heiles potential, the 3D coupled sextic oscillator, the scanned 4-cyano-2,2,6,6-tetramethyl-3,5-heptanedione H(1) potential and the 1D/2D/3D harmonic oscillator. The execution times for these examples may be several hours, depending on the method and the machine performance. An example script which processes the output is provided in the examples/visualization folder.

4. Conclusions

Three general purpose grid solvers for the bound 1D/2D/3D stationary Schrödinger equation were implemented and derived where appropriate. The implementations were validated against the chaotic Henon–Heiles potential and the 3D coupled sextic oscillators with accuracies matching those from reference literature values for the Chebyshev and DVR results. While the extension of the Numerov method to higher dimensions serves to illustrate the advantages of (pseudo)-spectral methods, the practical use for the method is likely to be limited. In contrast, the Chebyshev and DVR implementations provide a robust, efficient, and accurate tool for the calculation of three

Table A.1
H(1) DVR Eigenvalues — symmetric molecule. Energies for the first ten DVR eigenstates of the $H(1)$ atom in the symmetrized molecular structure are shown (left). Energies obtained from the Belot et al. [21] experimental structure (center) and the absolute energy difference between the two representations (right) are shown.

State	E_{DVR} symmetric (Hartree)	E_{DVR} of Table 2 (Hartree)	ΔE (kJ/mol)
E_0	0.008931791	0.0090415984	−0.3
E_1	0.013688026	0.0126778148	2.6
E_2	0.014530720	0.0146771085	−0.4
E_3	0.016915332	0.0167109298	0.5
E_4	0.018690721	0.0177493514	2.5
E_5	0.020202596	0.0193879520	2.1
E_6	0.021209330	0.0204142601	2.1
E_7	0.021510645	0.0207701462	1.9
E_8	0.022331278	0.0219828627	0.9
E_9	0.024159172	0.0230976863	2.8

Table A.2
Optimized structure of 4-cyano-2,2,6,6-tetramethyl-3,5-heptanedione. Coordinates from the optimized symmetric Z-matrix of 4-cyano-2,2,6,6-tetramethyl-3,5-heptanedione at the ωB97XD/6-31+G** level of theory, corrected for small numerical deviations.

Type	x (Å)	y (Å)	z (Å)
N	0.000	2.687	0.000
C	0.000	1.525	0.000
C	0.000	0.102	0.000
C	−1.229	−0.630	0.000
C	1.229	−0.630	0.000
O	−1.173	−1.902	0.000
O	1.173	−1.902	0.000
C	−2.624	−0.004	0.000
C	2.624	−0.004	0.000
C	−2.809	0.856	−1.267
C	2.809	0.856	1.267
C	−2.809	0.856	1.267
C	2.809	0.856	−1.267
C	−3.683	−1.116	0.000
C	3.683	−1.116	0.000
H	−2.719	0.261	2.180
H	2.719	0.261	2.180
H	−2.086	1.674	1.311
H	2.086	1.674	1.311
H	3.814	1.291	−1.251
H	3.814	1.291	1.251
H	−2.086	1.674	−1.311
H	2.086	1.674	−1.311
H	2.721	0.258	−2.179
H	−2.721	0.258	−2.179
H	−3.811	1.295	−1.251
H	−3.811	1.295	1.251
H	3.600	−1.758	−0.883
H	3.600	−1.758	0.883
H	−3.600	−1.758	−0.883
H	−3.600	−1.758	0.883
H	−4.675	−0.653	0.000
H	4.675	−0.653	0.000
H	−0.096	−2.145	0.000

dimensional nuclear wave functions. In practice, the errors between different DFT functionals will often be larger than the differences in the implemented solvers.

Acknowledgments

Appendix. Supporting information

We assessed the error of using the slightly asymmetric coordinates of Belot et al. [21] by optimizing the structure in an internal Z-matrix representation at the ωB97XD/6-31+G** level of theory prior to the potential scan. Beyond the optimization, all details of the calculation were as described in the manuscript. The barrier height of the symmetrized molecule is 0.3 kJ/mol compared to 2.6 kJ/mol obtained for the experimental coordinates (see Tables A.1 and A.2).

References

[1] L. Sobczyk, S.J. Grabowski, T.M. Krygowski, Interrelation between h-bond and pi-electron delocalization, Chem. Rev. 105 (10) (2005) 3513–3560.
[2] L. Wang, S.D. Fried, S.G. Boxer, T.E. Markland, Quantum delocalization of protons in the hydrogen-bond network of an enzyme active site, Proc. Natl. Acad. Sci. 111 (52) (2014) 18454–18459.
[3] A. Warshel, A. Papazyan, P.A. Kollman, On low-barrier hydrogen bonds and enzyme catalysis, Science 269 (5220) (1995) 102–106.
[4] K. Saito, H. Ishikita, Energetics of short hydrogen bonds in photoactive yellow protein, Proc. Natl. Acad. Sci. 109 (1) (2012) 167–172.
[5] K. Saito, H. Ishikita, Formation of an unusually short hydrogen bond in photoactive yellow protein, Bioenergetics 1827 (3) (2013) 387–394.
[6] S. Yamaguchi, H. Kamikubo, K. Kurihara, R. Kuroki, N. Niimura, N. Shimizu, Y. Yamazaki, M. Kataoka, Low-barrier hydrogen bond in photoactive yellow protein, Proc. Natl. Acad. Sci. 106 (2) (2009) 440–444.
[7] M. Nadal-Ferret, R. Gelabert, M. Moreno, J.M. Lluch, Are there really low-barrier hydrogen bonds in proteins? the case of photoactive yellow protein, J. Am. Chem. Soc. 136 (9) (2014) 3542–3552.
[8] A. Bulgac, M.M. Forbes, Use of the discrete variable representation basis in nuclear physics, Phys. Rev. C 87 (5) (2013) 051301.
[9] J.C. Light, T. Carrington Jr., Discrete-variable representations and their utilization, Adv. Chem. Phys. 114 (2000) 263–310.
[10] B.V. Numerov, Méthode nouvelle de la détermination des orbites et le calcul des éphémé rides en tenant compte des perturbations, Tr. Glavnoi Rossiik. Astrofizich. Obs. 2 (1923) 188.
[11] B. Noumerov, A method of extrapolation of perturbations, Mon. Not. R. Astron. Soc. 84 (1924) 592.
[12] M. Eckert, Solving the 1-, 2-, and 3-dimensional schrödinger equation for multiminima potentials using the numerov-cooley method. an extrapolation formula for energy eigenvalues, J. Comput. Phys. 82 (1) (1989) 147–160.
[13] Z. Kalogiratou, T. Monovasilis, T. Simos, Numerical solution of the two-dimensional time independent schrödinger equation with numerov-type methods, J. Math. Chem. 37 (3) (2005) 271–279.
[14] J.C. Mason, D.C. Handscomb, Chebyshev Polynomials, CRC Press, 2010.
[15] D.T. Colbert, W.H. Miller, A novel discrete variable representation for quantum mechanical reactive scattering via the s-matrix kohn method, J. Chem. Phys. 96 (3) (1992) 1982–1991.
[16] E. Polizzi, Density-matrix-based algorithm for solving eigenvalue problems, Phys. Rev. B 79 (11) (2009) 115112.
[17] E. Polizzi, A high-performance numerical library for solving eigenvalue problems: Feast solver v2. 1 user's guide, 2012. arXiv preprint arXiv:1203.4031.
[18] J. Cooley, An improved eigenvalue corrector formula for solving the schrödinger equation for central fields, Math. Comp. 15 (76) (1961) 363–374.
[19] B. Fornberg, A Practical Guide to Pseudospectral Methods, Vol. 1, Cambridge University Press, 1998.
[20] M. Braun, S. Sofianos, D. Papageorgiou, I. Lagaris, An efficient chebyshev–lanczos method for obtaining eigensolutions of the schrödinger equation on a grid, J. Comput. Phys. 126 (2) (1996) 315–327.
[21] J.A. Belot, J. Clark, J.A. Cowan, G.S. Harbison, A.I. Kolesnikov, Y.-S. Kye, A.J. Schultz, C. Silvernail, X. Zhao, The shortest symmetrical oh-o hydrogen bond has a low-barrier double-well potential, J. Phys. Chem. B 108 (22) (2004) 6922–6926.
[22] NIST Reference on Constants, Units, and Uncertainty. CODATA recommended values of the fundamental physical constants: 2014. http://physics.nist.gov/cuu/Constants/index.html, 2015. (accessed.07.15).
[23] J.-D. Chai, M. Head-Gordon, Systematic optimization of long-range corrected hybrid density functionals, J. Chem. Phys. 128 (8) (2008) 084106.
[24] J.-D. Chai, M. Head-Gordon, Long-range corrected hybrid density functionals with damped atom–atom dispersion corrections, Phys. Chem. Chem. Phys. 10 (44) (2008) 6615–6620.
[25] M.J. Frisch, G.W. Trucks, H.B. Schlegel, G.E. Scuseria, M.A. Robb, J.R. Cheeseman, G. Scalmani, V. Barone, B. Mennucci, G.A. Petersson, H. Nakatsuji, M. Caricato, X. Li, H.P. Hratchian, A.F. Izmaylov, J. Bloino, G. Zheng, J.L. Sonnenberg, M. Hada, M. Ehara, K. Toyota, R. Fukuda, J. Hasegawa, M. Ishida, T. Nakajima, Y. Honda, O. Kitao, H. Nakai, T. Vreven, J.A. Montgomery Jr., J.E. Peralta, F. Ogliaro, M. Bearpark, J.J. Heyd, E. Brothers, K.N. Kudin, V.N. Staroverov, R. Kobayashi, J. Normand, K. Raghavachari, A. Rendell, J.C. Burant, S.S. Iyengar, J. Tomasi, M. Cossi, N. Rega, J.M. Millam, M. Klene, J.E. Knox, J.B. Cross, V. Bakken, C. Adamo, J. Jaramillo, R. Gomperts, R.E. Stratmann, O. Yazyev, A.J. Austin, R. Cammi, C. Pomelli, J.W. Ochterski, R.L. Martin, K. Morokuma, V.G. Zakrzewski, G.A. Voth, P. Salvador, J.J. Dannenberg, S. Dapprich, A.D. Daniels, O. Farkas, J.B. Foresman, J.V. Ortiz, J. Cioslowski, D.J. Fox, Gaussian 09 Revision D.01, Gaussian Inc. Wallingford CT, 2009.
[26] J.C. Hargis, F.A. Evangelista, J.B. Ingels, H.F. Schaefer III, Short intramolecular hydrogen bonds: Derivatives of malonaldehyde with symmetrical substituents, J. Am. Chem. Soc. 130 (51) (2008) 17471–17478.